frontiers in Energy Research

ORIGINAL RESEARCH
published: 26 May 2015
doi: 10.3389/fenrg.2015.00025

Interfacial reaction dependent performance of hollow carbon nanosphere – sulfur composite as a cathode for Li-S battery

*Jianming Zheng[1], Pengfei Yan[1], Meng Gu[1], Michael J. Wagner[2], Kevin A. Hays[2], Junzheng Chen[1], Xiaohong Li[1], Chongmin Wang[1], Ji-Guang Zhang[1], Jun Liu[1] and Jie Xiao[1]**

[1] Pacific Northwest National Laboratory, Richland, WA, USA, [2] The George Washington University, Washington, DC, USA

Lithium-sulfur (Li-S) battery is a promising energy storage system due to its high energy density, cost effectiveness, and environmental friendliness of sulfur. However, there are still a number of technical challenges, such as low Coulombic efficiency and poor long-term cycle life, impeding the commercialization of Li-S battery. The electrochemical performance of Li-S battery is closely related with the interfacial reactions occurring between hosting substrate and active sulfur species, which are poorly conducting at fully oxidized and reduced states. Here, we correlate the relationship between the performance and interfacial reactions in the Li-S battery system, using a hollow carbon nanosphere (HCNS) with highly graphitic character as hosting substrate for sulfur. With an appropriate amount of sulfur loading, HCNS/S composite exhibits excellent electrochemical performance because of the fast interfacial reactions between HCNS and the polysulfides. However, further increase of sulfur loading leads to increased formation of highly resistive insoluble reaction products (Li_2S_2/Li_2S), which limits the reversibility of the interfacial reactions and results in poor electrochemical performances. These findings demonstrate the importance of the interfacial reaction reversibility in the whole electrode system on achieving high capacity and long cycle life of sulfur cathode for Li-S batteries.

Keywords: sulfur composite, interfacial reaction, sulfur utilization, cycling stability, rate capability, Li-S battery

OPEN ACCESS

Edited by:
Linda F. Nazar,
University of Waterloo, Canada

Reviewed by:
Lei Li,
Shanghai Jiao Tong University, China
Babak Shalchi Amirkhiz,
Natural Resources Canada, Canada

****Correspondence:***
Jie Xiao,
Energy and Environment Directorate, Pacific Northwest National Laboratory, 902 Battelle Boulevard, Richland, WA 99352, USA
jie.xiao@pnnl.gov

Specialty section:
This article was submitted to Energy Storage, a section of the journal Frontiers in Energy Research

Received: *20 January 2015*
Accepted: *09 May 2015*
Published: *26 May 2015*

Citation:
Zheng J, Yan P, Gu M, Wagner MJ, Hays KA, Chen J, Li X, Wang C, Zhang J-G, Liu J and Xiao J (2015) Interfacial reaction dependent performance of hollow carbon nanosphere – sulfur composite as a cathode for Li-S battery. Front. Energy Res. 3:25. doi: 10.3389/fenrg.2015.00025

Introduction

Lithium-sulfur (Li-S) batteries are attracting increasing worldwide attention because of their high theoretical capacity, natural abundance, low cost, and environmental friendliness (Mikhaylik and Akridge, 2004; Wang et al., 2008, 2015; Cao et al., 2011; Jayaprakash et al., 2011; Ji et al., 2011a,b; Zheng et al., 2011, 2013a,c,d,e; Schuster et al., 2012; Su and Manthiram, 2012a,b; Evers and Nazar, 2013; Huang et al., 2014; Xiao et al., 2015). Li-S battery operates by reduction of sulfur during discharge to form lithium polysulfides with different chain length and finally to produce Li_2S_2 or Li_2S. Assuming Li_2S as the final product, the maximum specific discharge capacity and energy from Li-S batteries are estimated to be 1675 Ah kg^{-1} and 2650 Wh kg^{-1}, respectively, three to five times higher than those of state-of-the-art lithium ion batteries (Xiao et al., 2012a; Zheng et al., 2013b). However, significant challenges have to be overcome prior to the practical application of Li-S battery. The low electrical conductivity of pure sulfur and the redox shuttle reaction of soluble

polysulfides between sulfur electrode and lithium anode are the main reasons for the low utilization rate of sulfur and poor electrochemical performances of Li-S battery, including low Coulombic efficiency, high self-discharge rate, and fast capacity fading (Mikhaylik and Akridge, 2004; Wang et al., 2008; Cao et al., 2011). To address the aforementioned hurdles in Li-S battery system, a variety of carbon frameworks, such as bimodal meso/microporous carbon (Liang et al., 2009), functionalized graphene sheet (Cao et al., 2011), mesoporous carbons (MPC) (Ji et al., 2011b, 2009; Chen et al., 2011; Jayaprakash et al., 2011; Li et al., 2011), hollow carbon nanofiber (Zheng et al., 2011), microporous carbon spheres (Zhang et al., 2010; Kim et al., 2013a), have been applied to enhance the electrochemical performance of sulfur electrodes. In addition, other organic materials such as polythiophene (Wu et al., 2010), polypyrrole (Fu and Manthiram, 2012), polyaniline (Xiao et al., 2012b), and metal organic framework (MOF) (Demir-Cakan et al., 2011; Zheng et al., 2014a) have also been adopted as sulfur hosting substrate and demonstrated to show good cycling performance.

Since the sulfur and its insoluble reaction products (Li_2S_2/Li_2S) are highly resistive in terms of ion conduction and electron conduction, the above mentioned strategies actually provide a favorable electrode interface for sulfur reduction and re-deposition of insoluble discharge products (Li_2S_2/Li_2S), which thus improves the utilization of sulfur and enhances the cycle life of the prepared sulfur cathodes. To further discuss the importance of the reversibility of interfacial reactions in Li-S battery, a hollow carbon nanosphere (HCNS) was adopted as hosting substrate because of its pronounced graphitic character, which could facilitate the efficient electron transport to the electrode interface to support the interfacial reactions between HCNS substrate and the polysulfides. The physical properties and electrochemical performance of the HCNS/S composites with different sulfur contents (50 and 80 wt% sulfur) were investigated in detail. The influence of sulfur content on the interfacial reactions between HCNS and the polysulfides was discussed in this work, which was thus correlated with the observed cell electrochemical performance.

Materials and Methods

Details for HCNS synthesis are described as reported previously (Zheng et al., 2013c). HCNS/S composite was prepared by a simple melt-diffusion method (Cao et al., 2011; Li et al., 2011). In brief, sulfur powder (Sigma–Aldrich) was first dissolved in carbon disulfide (CS_2) to form a 10 wt% solution. HCNS was added into sulfur-CS_2 solution. Then, the slurry was stirred under ambient temperature to evaporate CS_2. The obtained powder was grounded and heated at 155°C for 12 h in Teflon-lined stainless steel autoclave, to improve the sulfur distribution inside the carbon framework via capillary action. HCNS/S composites with 50 and 80% S were prepared. The accurate sulfur content was determined by the thermogravimetric analysis (TGA) with a Netzsch STA 449C thermal analysis system (Netzsch, Germany) from RT to 600°C at a heating rate of 10°C min^{-1} under N_2 flow. XRD was carried out on Panalytical X'Pert diffractometer (Holand) with Cu Kα radiation operated at 50 kV and 40 mA, and the XRD data were collected from 10° to 80° in 2θ at a step size of 0.04°. High resolution transmission electron microscopy (HRTEM) analysis was carried out on a JEOL JEM 2010 microscope fitted with a LaB6 filament and an acceleration voltage of 200 kV. Surface area, porosity, and pore size analysis were determined using nitrogen adsorption/desorption collected at 77 K with a QUANTACHROME AUTOSORB 6-B gas sorption system. The surface area was determined from the isotherm using 5 points Brunauer–Emmett–Teller (BET) method. Barrett-Joyner-Halenda (BJH) method was used for the porosity and pore size analysis. T method was used for micro pore analysis. Energy-dispersive X-ray spectroscopy (EDX) elemental mapping was investigated by JEOL JEM-ARM200CF microscope, which is operated at 200 kV and equipped with probe spherical aberration corrector, and a JEOL SDD-detector with a 100 mm^2 X-ray sensor.

Electrochemical measurements were carried out using CR2325 coin-type cell (Canadian National Research Council) system. Cathode electrodes were prepared by coating a mixture containing 80 wt% HCNS/S composite, 10 wt% super P (from Timcal), and 10 wt% poly(vinylidene fluoride) (Kynar HSV900, Arkema Inc.) binder onto Al current collector foil. The electrode loading is about 2 mg cm^{-2}. Coin cells were assembled with the HCNS/S cathode electrodes as-prepared, metallic lithium foil as counter electrode, Celgard 2400 microporous membrane as separator in an Argon-filled MBraun glove box. The electrolyte is 1M lithium bis(trifluoromethanesulfonyl)imide (LiTFSI) dissolved in a mixture of 1, 3-dioxolane (DOL) and dimethoxyethane (DME) (1:1 in volume). The sulfur/electrolyte ratio is controlled at 50 g L^{-1} (Zheng et al., 2013d). The electrochemical performance measurements were performed galvanostatically between 1.0 and 3.0 V at 0.2 and 0.5 C rates (1 C = 1680 mA g^{-1}) on an Arbin BT-2000 battery tester at room temperature. The rate capability was evaluated with a constant charge at 0.2 C, and a gradual ascending in the discharge C rate after initial five charge/discharge cycles at 0.1 C. The capacity is calculated based on the active sulfur component of the HCNS/S composite. Cyclic voltammetry (CV) was performed on a CHI 6005D electrochemical station (from CH Instruments) between 1.0 and 3.0 V at a scan rate of 0.2 mV s^{-1}. Electrochemical Impedance Spectra (EIS) measurements were performed using the CHI 6005D electrochemical station in a frequency range from 100 kHz to 10 mHz with a perturbation amplitude of ±10 mV.

Results and Discussion

Figure 1 shows the N_2 adsorption–desorption isotherms and pore size distribution of pristine HCNS and HCNS/S composites. As summarized in **Table 1**, the pristine HCNS has a BET surface area of 75.5 m^2 g^{-1} with a pore volume of 0.379 cm^3 g^{-1}, which could accommodate 44.0 wt% of sulfur inside the pores. To investigate the influence of sulfur content on the interfacial reactions and the consequent electrochemical performance of Li-S battery, HCNS/S composites with different sulfur loading were prepared: one is loaded with sulfur content of 50 wt% S (indicated as HCNS/S50), which is close to the maximum limit as determined by the pore volume of HCNS, while the other one is loaded with significantly excessive sulfur content (80 wt% S) (indicated as HCNS/S80).

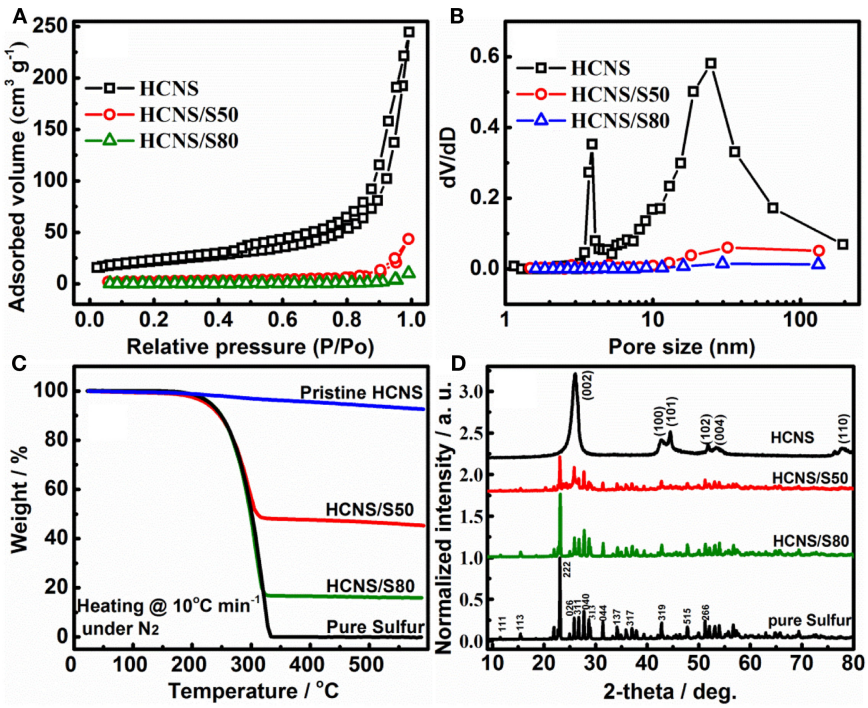

FIGURE 1 | (A) N_2 adsorption/desorption isotherms; **(B)** pore size distribution; **(C)** TGA curves; and **(D)** XRD patterns of the pure S, pristine HCNS, and HCNS/S composites: the XRD patterns of S and HCNS/S composites were normalized over the intensity of the (222) peak of the S; the XRD pattern of HCNS was normalized over its maximum intensity (002) peak for comparison.

TABLE 1 | BET results and electrochemical performance of HCNS/S composites.

	HCNS	HCNS/S50	HCNS/S80
Surface area / $m^2\ g^{-1}$	75.5	8.38	1.88
Pore volume / $cm^3\ g^{-1}$	0.379	0.067	0.016
Initial capacity at 0.2 C / mAh g^{-1}	–	1170	774
Capacity after 100 cycles at 0.2 C / mAh g^{-1}	–	754	484

After sulfur impregnation, both HCNS/S composites show largely reduced BET surface area and pore volume (**Table 1**), as evidenced by the decrease of hysteresis loop in isotherms (**Figure 1A**) and the diminishing pore size distribution profile (**Figure 1B**). The reduced surface area after sulfur loading could be partially due to the sulfur covering on the outer surface blocking the access of N_2 to inner surface of the HCNS. Another more important reason is that sulfur melted and diffused into the hollow pores of HCNS during heat treatment leading to the significant decrease of surface area. The accurate loading content of sulfur was confirmed by the TGA measurement (**Figure 1C**). XRD patterns of the pure sulfur, pristine HCNS, and HCNS/S composites are shown in **Figure 1D**. As shown, the HCNS carbon framework shows sharp crystalline peaks of carbon, suggesting that HCNS contains high graphitic content and allows fast transport of electrons to/from the poorly conducting active materials, including sulfur and polysulfides (Jayaprakash et al., 2011). The elemental sulfur and HCNS/S composites show XRD peaks that could be assigned to those of pure orthorhombic sulfur (PDF no. 00-008-0247) (Su and Manthiram, 2012b).

The TEM images of HCNS, HCNS/S50, and HCNS/S80 are shown in **Figures 2A–C**, respectively. Visually, the HCNS is mainly composed of large mesopores with pore size ranging from 10 to 50 nm and well crystallized carbon wall of ca. 10 nm, in well accordance with the pore size distribution analysis and XRD result. The enclosed large mesopores of HCNS is attractive because they could potentially trap the polysulfides produced from the Li-S redox reactions, thus affording good cycling performance of HCNS/S composite. **Figure 2D** presents the HRTEM image of HCNS carbon wall, which exhibits highly graphitic character. Elemental mapping of C and S was further carried out to understand how the S element distributes in the HCNS/S composite, as shown in **Figure 3**. It can be seen that sulfur distributes homogeneously throughout the carbon nanosphere framework. The two intensity profiles in the **Figure 3D** show that some of the sulfur melted and was absorbed by the HCNS carbon substrate during the heat treatment at 155°C. A significant quantity of the sulfur just covers on the outer surface of HCNS carbon walls. The EDX maps also show that sulfur only exists where carbon substrate is identified, and there is no obviously segregated sulfur detected. The intimate contact between sulfur and the carbon substrate, and the fast transport of electrons in the graphitic carbon matrix will readily facilitate the electrochemical interfacial reactions between HCNS framework and polysulfides both at outer surface and at inner surface.

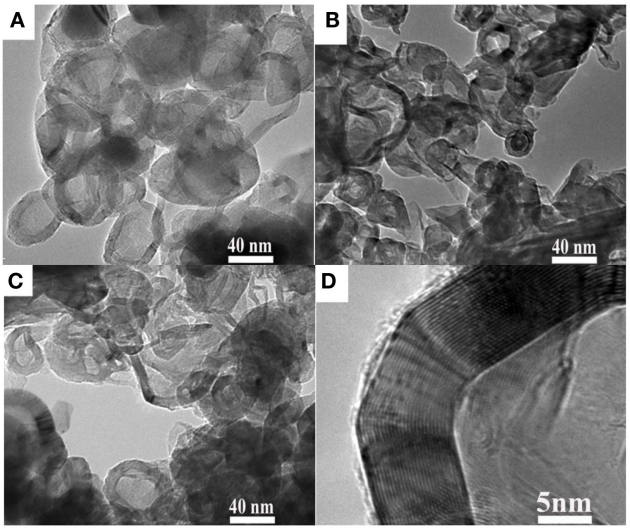

FIGURE 2 | TEM images of (A) pristine HCNS, (B) HCNS/S50 composite, and (C) HCNS/S80 composite. (D) HRTEM image of HCNS carbon wall showing highly graphitic character.

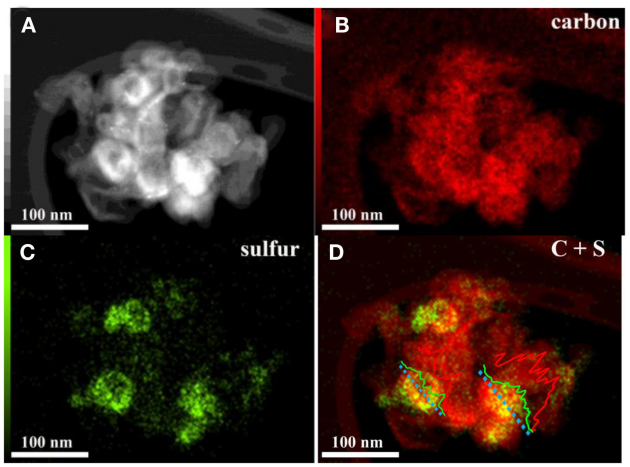

FIGURE 3 | (A) HAADF Z-contrast image; **(B)** carbon and **(C)** sulfur EDX maps; **(D)** overlaid C/S map of HCNS/S50 composite material. Inset in **(D)** are the intensity profiles of carbon and sulfur across the HCNS/S composite nano particles.

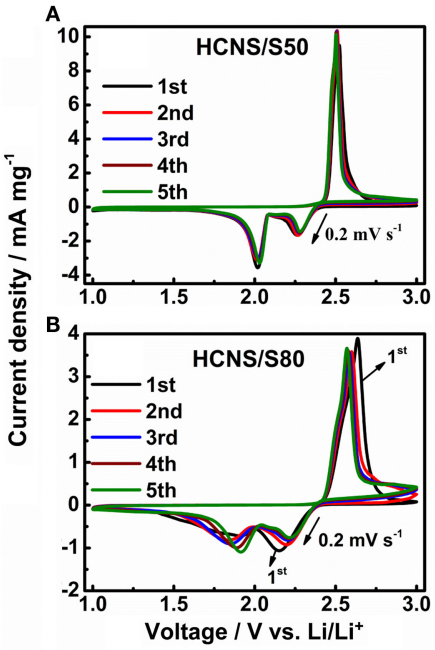

FIGURE 4 | Cyclic voltammograms (CV) of HCNS/S composite cathodes at 0.2 mV s^{-1}. (A) HCNS/S50 composite, **(B)** HCNS/S80 composite.

To understand the redox reactions of the HCNS/S composites in Li-S batteries, CV tests were conducted with CR2325 coin-type cells at a scan rate of 0.2 mV s^{-1}, and the results are shown in **Figure 4**. For HCNS/S50 composite, two typical reduction peaks at around 2.30 and 2.05 V are well-resolved during the cathodic scan, corresponding to a two-step reduction of sulfur. The first step at ca. 2.3 V corresponds to the conversion of sulfur to high-order polysulfides (Li_2S_n, $4 \leq n < 8$). The second step is ascribed to further transformation of high-order polysulfides to low-order polysulfides (Li_2S_n, $n < 4$), and finally to insoluble lithium sulfide (Li_2S_2/Li_2S) (Wu et al., 2010). It is worth to note that there is a minor reduction peak between the two main reduction peaks, due to the formation of S_6^{2-} and S_4^{2-} from S_8^{2-}/S_8 (Cao et al., 2011). In the subsequent anodic scan, the sharp oxidation peak at about 2.5 V is attributed to the conversion of low-order polysulfides back to high-order polysulfides and then the intermediate S_8^{2-}. During the following cycles, both cathodic and anodic peaks remain stable in terms of current and potential, indicating that the interfacial reactions between HCNS and the polysulfides are highly reversible with low kinetic barrier. While for the HCNS/S80 composite, because of the reduced content of HCNS, there are not enough carbon surfaces dedicated for the reversible interfacial reactions between HCNS and the polysulfides, especially for the re-deposition of insoluble reduced products Li_2S_2/Li_2S back onto the HCNS surface. Therefore, the HCNS/S80 composite shows redox peaks distributing in a broad voltage range because of the increasing cell polarization. The HCNS/S80 composite also shows increased current response at high voltage region (2.75 ~ 3.0 V) during subsequent scans, indicating an increase of shuttling effect and a reduced Coulombic efficiency.

The electrochemical performances of the HCNS/S composites were further evaluated using galvanostatic charge/discharge protocol, and the results are shown in **Figure 5**. **Figure 5A** shows the typical charge/discharge profiles for HCNS/S composites at 0.2 C (336 mA g^{-1}). The two discharge voltage plateaus are in good agreement with the reduction peaks observed in the CV scans. The upper voltage plateau at ca. 2.3 V corresponds to the transition from S_8 to long chain polysulfides (Li_2S_8, Li_2S_6 or Li_2S_4), while the lower one at ca. 2.1 V reflects the further reduction of Li_2S_4 to lower order series of Li_2S_2/Li_2S (Jayaprakash et al., 2011; Zheng et al., 2011). The two HCNS/S composites show similar discharge capacity of upper voltage plateau at ca. 2.3 V, as reflected by the overlapped discharge profile above 2.1 V (Point *A*). However, the lower voltage plateau at 2.1 becomes largely shortened and

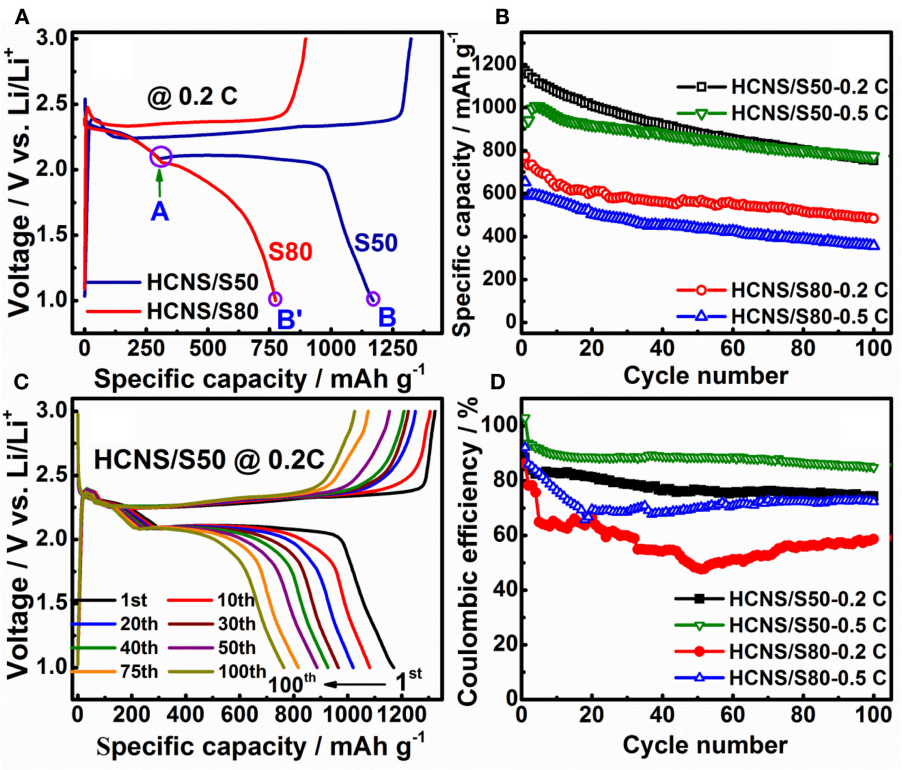

FIGURE 5 | (A) Charge/discharge profiles of HCNS/S composites at 0.2 C (336 mA g^{-1}). **(B)** Cycling performance of the HCNS/S composites. **(C)** Charge/discharge profile evolution of HCNS/S50 composite during cycling at 0.2 C. **(D)** Comparison of Coulombic efficiency of the HCNS/S composites.

the cell polarization increases dramatically with the increase of sulfur loading, revealing a decrease of conversion reaction from long chain polysulfides to insoluble Li_2S_2/Li_2S (decreased from Point *B* to *B*′). This is because the interfacial reactions from solid sulfur to liquid polysulfides occurring at 2.3 V is kinetically faster than the interfacial reactions from liquid polysulfides to solid (Li_2S_2/Li_2S) reaction initiating at lower plateau (~2.1 V). Although a redistribution of polysulfides among the whole electrode is unavoidable once discharge process is initiated, with high sulfur loading (80% S), the HCNS carbon framework could not provide enough surface area for re-deposition of insoluble reduction products (Li_2S_2/Li_2S) back onto the carbon surface. As a consequence, HCNS/S80 also shows much higher cell polarization during subsequent charge process because of the formation of thick film of poorly conducting discharge products on carbon surface.

Figure 5B compares the cycling performances of HCNS/S composites with different sulfur loading. The result indicates that the sulfur utilization is dependent on the interfacial reactions that occur between HCNS and the reduced polysulfides. At high sulfur loading, HCNS/S80 composite only delivers 774 mAh g^{-1} at 0.2 C, corresponding to a low sulfur utilization of 46.2%. On the contrary, with appropriate sulfur content the HCNS/S50 composite exhibits much higher discharge capacity of 1170 mAh g^{-1} at 0.2 C, corresponding to greatly improved sulfur utilization (69.6%). After 100 cycles, the HCNS/S50 composite still retains capacities of 754 and 772 mAh g^{-1} at 0.2 and 0.5 C, respectively, much higher than 484 and 356 mAh g^{-1} for the HCNS/S80 composite. Meanwhile, the charge/discharge plateaus maintain relatively stable during cycling, as shown in **Figure 5C**, confirming the excellent cycling performance of HCNS/S50 composite. That is because with appropriate sulfur loading, the deposition of thick layer of discharge products (Li_2S_2/Li_2S) could be avoided or alleviated, thus leading to good cycling performance (Zheng et al., 2013c). With excessive sulfur loading, the thick layer of discharge products (Li_2S_2/Li_2S) is difficult to get completely oxidized, resulting in continuous accumulation of dead Li_2S in the cycled electrode and leading to fast capacity fading. It is worth to note that the lower voltage plateau at ca. 2.1 V shrinks significantly during cycling, while the upper voltage plateau at ca. 2.3 V keeps relatively stable. This implies that the active surface of HCNS is gradually deactivated due to the passivation of insulating Li_2S/Li_2S_2, which dramatically increases the kinetic barrier for the interfacial reactions between HCNS and polysulfides. This may be also one of the main reasons contributing to the continuous capacity fading of other Li-S battery systems. The charge/discharge performance as reported for HCNS/S50 composite is comparable to or superior over those reported for C/S composites with similar sulfur loading and using normal electrolyte without $LiNO_3$ additive (Liang et al., 2009; Elazari et al., 2011; Li et al., 2011; Kim et al., 2013a; Weng et al., 2013; Wang et al., 2014; Zhao et al., 2014). The discharge capacity of HCNS/S50 composite cathode is calculated to be 468 mAh g^{-1} based on the whole electrode, and the energy density is determined to be 948 Wh kg^{-1}. This energy density value is still higher than the lithium-rich manganese-rich cathode material for

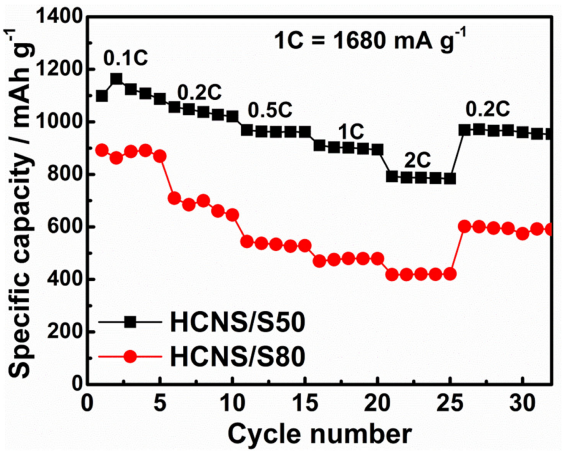

FIGURE 6 | Rate performance of HCNS/S composites with different sulfur loading (1 C = 1680 mA g^{-1}).

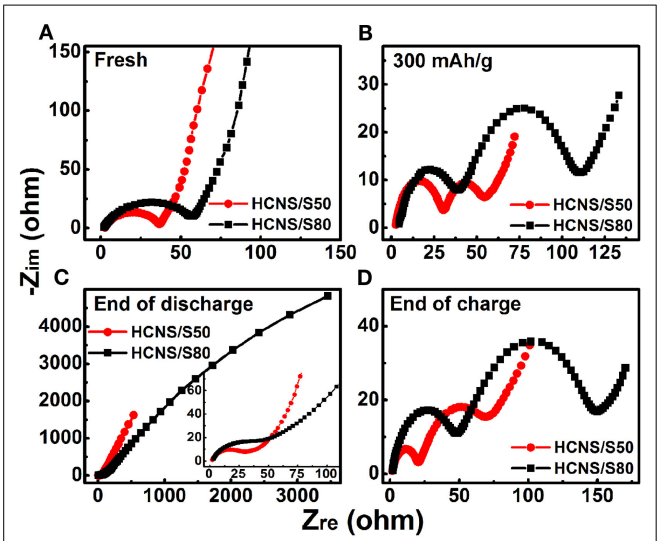

FIGURE 7 | Evolution of impedance spectra of cells with different HCNS/S composite electrodes during initial discharge/charge processes. (A) Before cycling; **(B)** discharge to a capacity of 300 mAh g^{-1}; **(C)** end of discharge (inset is enlarged from high-medium frequency region); **(D)** end of charge.

LIBs, which delivers the highest gravimetric energy density among the cathode candidates for LIBs (about 900 Wh kg^{-1}) (Zheng et al., 2014b,c, 2015).

Figure 5D presents the Coulombic efficiencies of these two HCNS/S composites during cycling at 0.2 and 0.5 C rates. On the one hand, the Coulombic efficiency of HCNS/S composite is increased with the increase of charge/discharge current density, ascribed to reduced time for polysulfides to migrate to lithium metal anode. On the other hand, the Coulombic efficiency is dependent on the sulfur loading in the composite material. With excessive sulfur loading, the HCNS/S80 composite generally shows relatively low Coulombic efficiency at different C rates, which is expected because the sluggish interfacial reactions between limited HCNS and the higher content of polysulfides could not timely re-oxidize all of the lower-order polysulfides to higher-order polysulfides, leading to more obvious shuttling. The decreased Coulombic efficiency is consistent with the increased current response as observed in the CV scans (**Figure 4B**). In addition, due to the increased shuttling effect, more of the high-order polysulfides are irreversibly reduced to form insoluble Li_2S_2/Li_2S on lithium metal surface, leading to increase of cell resistance and fast capacity fading (**Figure 5B**). With appropriate sulfur loading, the HCNS/S50 composite shows significantly improved Coulombic efficiencies during long-term cycling both at 0.2 and 0.5 C as compared to those of HCNS/S80 composite. The high Coulombic efficiency of HCNS/S50 composite is attributed to the fast interfacial reactions occurring between the relatively higher content of HCNS and polysulfides during charge process that reduces the undesirable shuttling reactions.

Rate capabilities of the two HCNS/S composites were further evaluated, and the result is illustrated in **Figure 6**. The discharge capacity decrease with the increase of current rate ascribed to the increase of cell polarization and decrease of interfacial reactions at higher C rates. The HCNS/S50 composite shows relatively high discharge capacities at different C rates, delivering 910 mAh g^{-1} at 1 C and 792 mAh g^{-1} at 2 C, which are considerably higher than 470 and 418 mAh g^{-1} for HCNS/S80 composite. The good rate capability of HCNS/S50 composite could be ascribed to the high graphitic character of HCNS, which facilitates the timely electron transfer to/from orly conducting S and polysulfides and hence ensures the fast interfacial reactions between HCNS and active S species in the electrode system. However, further increase of sulfur content (decrease of HCNS content) readily retards these interfacial reactions, resulting in reduced discharge capacities at different C rates. This result further demonstrates the relationship between the rate performance and the interfacial reactions that occur in Li-S battery systems.

To further understand the performance difference of different HCNS/S composite cathodes, EIS measurements were performed to study the cell impedance evolution during initial dis/charge processes, and the results are presented in **Figure 7**. Before cycling, the semicircle observed in the high-medium frequency region is a combination of surface film resistance and charge transfer resistance (**Figure 7A**) (Zheng et al., 2014a). After discharge to a capacity of 300 mAh g^{-1} (Point A of **Figure 5A**), a high-frequency semicircle, an intermediate-frequency semicircle and low-frequency tails are observed (**Figure 7B**), because of the formation of soluble polysulfides in the electrolyte. Although the detailed assignment in the Nyquist plot is still controversial for Li-S batteries, it is generally interpreted that the high-frequency semicircle is related with the surface film resistance (R_{sf}), the intermediate-frequency semicircle is ascribed to the charge transfer resistance (R_{ct}) in the electrode/electrolyte interface, while the low-frequency tail is associated with the Li^+ ion diffusion process in the solid electrode (Kim et al., 2013b). At the end of discharge, serious Warburg impedance is detected at the low frequency range due to the accumulation of insoluble discharge products Li_2S_2/Li_2S (**Figure 7C**), indicating a large kinetic barrier at the completion of discharge. At the end of charge, two semicircles appear (**Figure 7D**) because the discharge products Li_2S_2/Li_2S are converted back to soluble polysulfides and then to sulfur

$\left(S_4^{2-}/S_8\right)$. From comparison, it is found that the HCNS/S50 composite always shows lower cell resistances (surface film resistance and charge transfer resistance) during electrochemical reaction processes. The lower resistances of cell with higher content of HCNS (HCNS/S50) are conducive to enhance the electrochemical interfacial reactions during dis/charge process, which enables the superior long-term cycling performance and rate capability. The EIS result is in good agreement with the above discussion on the relationship between interfacial reactions and the electrochemical performance of Li-S batteries.

Conclusion

Hollow carbon nanosphere-sulfur composites have been investigated as cathode materials for Li-S battery, and the electrochemical performances were correlated with the interfacial reactions occurring in the whole electrode system. With an appropriate content of sulfur loading (50 wt% S), HCNS/S composite shows a high discharge capacity of 1170 mAh g^{-1} at 0.2 C and good cycling stability as well as decent rate performance, ascribed to the fast interfacial reactions between HCNS and the polysulfides. However, excessive sulfur loading leads to increased formation of highly resistive insoluble reaction products (Li_2S_2/Li_2S), which limits the reversibility of the interfacial reactions and results in poor electrochemical performance including low sulfur utilization rate and fast capacity fading. It is expected that further optimizing the microstructure of HCNS framework that could facilitate the reversible interfacial reactions would allow to increase the sulfur loading, and thus improve the energy density of the whole electrode.

Acknowledgments

This work was supported by the Assistant Secretary for Energy Efficiency and Renewable Energy, Office of Vehicle Technologies of the U.S. Department of Energy (DOE) under Contract No. DEAC02-05CH11231 for PNNL and under DEAC02-98CH10886 under the Battery Material Research (BMR) program. TEM and EDX analysis were conducted at the Environmental and Molecular Sciences Laboratory, a national scientific user facility sponsored by the Department of Energy's Office of Biological and Environmental Research and located at Pacific Northwest National Laboratory. PNNL is a multi-program national laboratory operated for DOE by Battelle under Contract DE AC05-76RL01830.

Supplementary Material

The Supplementary Material for this article can be found online at http://journal.frontiersin.org/article/10.3389/fenrg.2015.00025

References

Cao, Y., Li, X., Aksay, I. A., Lemmon, J., Nie, Z., Yang, Z., et al. (2011). Sandwich-type functionalized graphene sheet-sulfur nanocomposite for rechargeable lithium batteries. *Phys. Chem. Chem. Phys.* 13, 7660–7665. doi:10.1039/C0CP02477E

Chen, S.-R., Zhai, Y.-P., Xu, G.-L., Jiang, Y.-X., Zhao, D.-Y., Li, J.-T., et al. (2011). Ordered mesoporous carbon/sulfur nanocomposite of high performances as cathode for lithium-sulfur battery. *Electrochim. Acta* 56, 9549–9555. doi:10.1016/j.electacta.2011.03.005

Demir-Cakan, R., Morcrette, M., Nouar, F., Davoisne, C., Devic, T., Gonbeau, D., et al. (2011). Cathode composites for Li-S batteries via the use of oxygenated porous architectures. *J. Am. Chem. Soc.* 133, 16154–16160. doi:10.1021/ja2062659

Elazari, R., Salitra, G., Garsuch, A., Panchenko, A., and Aurbach, D. (2011). Sulfur-impregnated activated carbon fiber cloth as a binder-free cathode for rechargeable Li-S batteries. *Adv. Mater.* 23, 5641–5644. doi:10.1002/adma.201103274

Evers, S., and Nazar, L. F. (2013). New approaches for high energy density lithium-sulfur battery cathodes. *Acc. Chem. Res.* 46, 1135–1143. doi:10.1021/ar3001348

Fu, Y., and Manthiram, A. (2012). Orthorhombic bipyramidal sulfur coated with polypyrrole nanolayers as a cathode material for lithium-sulfur batteries. *J. Phys. Chem. C* 116, 8910–8915. doi:10.1021/jp300950m

Huang, C., Xiao, J., Shao, Y., Zheng, J., Bennett, W. D., Lu, D., et al. (2014). Manipulating surface reactions in lithium-sulphur batteries using hybrid anode structures. *Nat. Commun.* 5, 3015. doi:10.1038/ncomms4015

Jayaprakash, N., Shen, J., Moganty, S. S., Corona, A., and Archer, L. A. (2011). Porous hollow carbon@sulfur composites for high-power lithium-sulfur batteries. *Angew. Chem. Int. Ed.* 50, 5904–5908. doi:10.1002/anie.201100637

Ji, L., Rao, M., Zheng, H., Zhang, L., Li, Y., Duan, W., et al. (2011a). Graphene oxide as a sulfur immobilizer in high performance lithium/sulfur cells. *J. Am. Chem. Soc.* 133, 18522–18525. doi:10.1021/ja206955k

Ji, X., Evers, S., Black, R., and Nazar, L. F. (2011b). Stabilizing lithium-sulphur cathodes using polysulphide reservoirs. *Nat. Commun.* 2, 325. doi:10.1038/ncomms1293

Ji, X., Lee, K. T., and Nazar, L. F. (2009). A highly ordered nanostructured carbon-sulphur cathode for lithium-sulphur batteries. *Nat. Mater.* 8, 500–506. doi:10.1038/nmat2460

Kim, J., Lee, D.-J., Jung, H.-G., Sun, Y.-K., Hassoun, J., and Scrosati, B. (2013a). An advanced lithium-sulfur battery. *Adv. Funct. Mater.* 23, 1076–1080. doi:10.1002/adfm.201200689

Kim, C. S., Guerfi, A., Hovington, P., Trottier, J., Gagnon, C., Barray, F., et al. (2013b). Importance of open pore structures with mechanical integrity in designing the cathode electrode for lithium-sulfur batteries. *J. Power Sources* 241, 554–559. doi:10.1016/j.jpowsour.2013.05.026

Li, X., Cao, Y., Qi, W., Saraf, L. V., Xiao, J., Nie, Z., et al. (2011). Optimization of mesoporous carbon structures for lithium-sulfur battery applications. *J. Mater. Chem.* 21, 16603–16610. doi:10.1039/C1JM12979A

Liang, C., Dudney, N. J., and Howe, J. Y. (2009). Hierarchically structured sulfur/carbon nanocomposite material for high-energy lithium battery. *Chem. Mater.* 21, 4724–4730. doi:10.1021/cm902050j

Mikhaylik, Y. V., and Akridge, J. R. (2004). Polysulfide shuttle study in the Li/S battery system. *J. Electrochem. Soc.* 151, A1969–A1976. doi:10.1149/1.1806394

Schuster, J., He, G., Mandlmeier, B., Yim, T., Lee, K. T., Bein, T., et al. (2012). Spherical ordered mesoporous carbon nanoparticles with high porosity for lithium-sulfur batteries. *Angew. Chem. Int. Ed.* 51, 3591–3595. doi:10.1002/anie.201107817

Su, Y.-S., and Manthiram, A. (2012a). Lithium-sulphur batteries with a microporous carbon paper as a bifunctional interlayer. *Nat. Commun.* 3, 1166. doi:10.1038/ncomms2163

Su, Y.-S., and Manthiram, A. (2012b). A facile in situ sulfur deposition route to obtain carbon-wrapped sulfur composite cathodes for lithium-sulfur batteries. *Electrochim. Acta* 77, 272–278. doi:10.1016/j.electacta.2012.06.002

Wang, J., Chew, S. Y., Zhao, Z. W., Ashraf, S., Wexler, D., Chen, J., et al. (2008). Sulfur-mesoporous carbon composites in conjunction with a novel ionic liquid electrolyte for lithium rechargeable batteries. *Carbon N. Y.* 46, 229–235. doi:10.1016/j.carbon.2007.11.007

Wang, L., Zhao, Y., Thomas, M. L., and Byon, H. R. (2014). In situ synthesis of bipyramidal sulfur with 3D carbon nanotube framework for lithium-sulfur batteries. *Adv. Funct. Mater.* 24, 2248–2252. doi:10.1002/adfm.201302915

Wang, Q., Zheng, J., Walter, E., Pan, H., Lv, D., Zuo, P., et al. (2015). Direct observation of sulfur radicals as reaction media in lithium sulfur batteries. *J. Electrochem. Soc.* 162, A474–A478. doi:10.1149/2.0851503jes

Weng, W., Pol, V. G., and Amine, K. (2013). Ultrasound assisted design of sulfur/carbon cathodes with partially fluorinated ether electrolytes for highly efficient Li/S batteries. *Adv. Mater.* 25, 1608–1615. doi:10.1002/adma.201204051

Wu, F., Wu, S., Chen, R., Chen, J., and Chen, S. (2010). Sulfur-polythiophene composite cathode materials for rechargeable lithium batteries. *Electrochem. Solid State Lett.* 13, A29–A31. doi:10.1149/1.3290668

Xiao, J., Chen, X., Sushko, P. V., Sushko, M. L., Kovarik, L., Feng, J., et al. (2012a). High-performance $LiNi_{0.5}Mn_{1.5}O_4$ spinel controlled by Mn^{3+} concentration and site disorder. *Adv. Mater.* 24, 2109–2116. doi:10.1002/adma.201104767

Xiao, L., Cao, Y., Xiao, J., Schwenzer, B., Engelhard, M. H., Saraf, L. V., et al. (2012b). A soft approach to encapsulate sulfur: polyaniline nanotubes for lithium-sulfur batteries with long cycle life. *Adv. Mater.* 24, 1176–1181. doi:10.1002/adma.201103392

Xiao, J., Hu, J. Z., Chen, H., Vijayakumar, M., Zheng, J., Pan, H., et al. (2015). Following the transient reactions in lithium-sulfur batteries using an in situ nuclear magnetic resonance (NMR) technique. *Nano Lett.* 15, 3309–3316. doi:10.1021/acs.nanolett.5b00521

Zhang, B., Qin, X., Li, G. R., and Gao, X. P. (2010). Enhancement of long stability of sulfur cathode by encapsulating sulfur into micropores of carbon spheres. *Energy Environ. Sci.* 3, 1531–1537. doi:10.1039/C002639E

Zhao, X., Kim, D.-S., Manuel, J., Cho, K.-K., Kim, K.-W., Ahn, H.-J., et al. (2014). Recovery from self-assembly: a composite material for lithium-sulfur batteries. *J. Mater. Chem. A* 2, 7265–7271. doi:10.1039/C4TA00490F

Zheng, G., Yang, Y., Cha, J. J., Hong, S. S., and Cui, Y. (2011). Hollow carbon nanofiber-encapsulated sulfur cathodes for high specific capacity rechargeable lithium batteries. *Nano Lett.* 11, 4462–4467. doi:10.1021/nl2027684

Zheng, J., Gu, M., Chen, H., Meduri, P., Engelhard, M. H., Zhang, J.-G., et al. (2013a). Ionic liquid-enhanced solid state electrolyte interface (SEI) for lithium-sulfur batteries. *J. Mater. Chem. A* 1, 8464–8470. doi:10.1039/C3TA11553D

Zheng, J., Xiao, J., Nie, Z., and Zhang, J.-G. (2013b). Lattice Mn^{3+} behaviors in $Li_4Ti_5O_{12}/LiNi_{0.5}Mn_{1.5}O_4$ full cells. *J. Electrochem. Soc.* 160, A1264–A1268. doi:10.1149/2.097308jes

Zheng, J., Gu, M., Wagner, M. J., Hays, K. A., Li, X., Zuo, P., et al. (2013c). Revisit carbon/sulfur composite for Li-S batteries. *J. Electrochem. Soc.* 160, A1624–A1628. doi:10.1149/2.013310jes

Zheng, J., Lv, D., Gu, M., Wang, C., Zhang, J.-G., Liu, J., et al. (2013d). How to obtain reproducible results for lithium sulfur batteries? *J. Electrochem. Soc.* 160, A2288–A2292. doi:10.1149/2.106311jes

Zheng, J., Gu, M., Wang, C., Zuo, P., Koech, P. K., Zhang, J.-G., et al. (2013e). Controlled nucleation and growth process of Li_2S_2/Li_2S in lithium-sulfur batteries. *J. Electrochem. Soc.* 160, A1992–A1996. doi:10.1149/2.032311jes

Zheng, J., Tian, J., Wu, D., Gu, M., Xu, W., Wang, C., et al. (2014a). Lewis acid-base interactions between polysulfides and metal organic framework in lithium sulfur batteries. *Nano Lett.* 14, 2345–2352. doi:10.1021/nl404721h

Zheng, J., Gu, M., Genc, A., Xiao, J., Xu, P., Chen, X., et al. (2014b). Mitigating voltage fade in cathode materials by improving the atomic level uniformity of elemental distribution. *Nano Lett.* 14, 2628–2635. doi:10.1021/nl500486y

Zheng, J., Xiao, J., Gu, M., Zuo, P., Wang, C., and Zhang, J.-G. (2014c). Interface modifications by anion receptors for high energy lithium ion batteries. *J. Power Sources* 250, 313–318. doi:10.1016/j.jpowsour.2013.10.071

Zheng, J., Xu, P., Gu, M., Xiao, J., Browning, N. D., Yan, P., et al. (2015). Structural and chemical evolution of Li- and Mn-rich layered cathode material. *Chem. Mater.* 27, 1381–1390. doi:10.1021/cm5045978

Conflict of Interest Statement: The authors declare that the research was conducted in the absence of any commercial or financial relationships that could be construed as a potential conflict of interest.